Electronic structure trends in the $Sr_{n+1}Ru_nO_{3n+1}$ family ($n = 1,2,3$)

M. Malvestuto,[1] E. Carleschi,[2,3,*] R. Fittipaldi,[4,5] E. Gorelov,[6] E. Pavarini,[6,†] M. Cuoco,[4,5,‡] Y. Maeno,[7] F. Parmigiani,[2,3] and A. Vecchione[4,5]

[1]*Sincrotrone Trieste, Area Science Park, I-34012 Basovizza, Trieste, Italy*
[2]*CNR-IOM, TASC Laboratory, Area Science Park, I-34012 Basovizza, Trieste, Italy*
[3]*Dipartimento di Fisica, Università degli Studi di Trieste, I-34127 Trieste, Italy*
[4]*CNR-SPIN, I-84084 Fisciano, Salerno, Italy*
[5]*Dipartimento di Fisica "E.R. Caianiello," Università di Salerno, I-84084 Fisciano, Salerno, Italy*
[6]*Institut für Festkörperforschung and Institute for Advanced Simulation, Forschungszentrum Jülich, D-52425 Jülich, Germany*
[7]*Department of Physics, Kyoto University, Kyoto 606-8502, Japan*

(Received 27 January 2011; published 19 April 2011)

The identification of electronic states and the analysis of their evolution with n is key to understanding n-layered ruthenates. To this end, we combine polarization-dependent O 1s x-ray absorption spectroscopy, high-purity $Sr_{n+1}Ru_nO_{3n+1}$ ($n = 1,2,3$) single crystals, and *ab initio* and many-body calculations. We find that the energy splitting between the empty $x^2 - y^2$ and $3z^2 - 1$ state is considerably smaller than previously suggested and that, remarkably, Sr bands are essential to understanding the spectra. At low energy, we identify the main difference among the materials with a substantial rearrangement of t_{2g} orbital occupations with increasing n. This rearrangement is controlled by the interplay of Coulomb repulsion, dimensionality, and changes in the t_{2g} crystal field.

DOI: 10.1103/PhysRevB.83.165121 PACS number(s): 71.20.Be, 71.15.−m, 71.27.+a, 78.70.Dm

I. INTRODUCTION

The ruthenates of the Ruddlesden-Popper family $A_{n+1}Ru_nO_{3n+1}$ (A = Ca and Sr) (Fig. 1) are unique among transition-metal oxides because the change in the number n of RuO_2 layers leads to a variety of collective phenomena: spin-triplet chiral superconductivity[3] and Fermi-surface anomalies[4] ($n = 1$); heavy d-electron masses[5–8] ($n = 1,2$); colossal magnetoresistance,[9] proximity to a metamagnetic quantum critical point, and nematic fluid behavior[10–12] ($n = 2$); and itinerant ferromagnetism and metamagnetism ($n = 3$).[13–15] It is believed that such diversity stems from the interplay of orbital, spin, and lattice degrees of freedom in the partially filled Ru 4d shells ($t_{2g}^4 e_g^0$). Understanding how the change in n, which reflects the dimensionality, modifies this interplay is thus crucial to explaining the physics of these ruthenates.

Single-layered ($n = 1$) systems are regarded as quasi-two-dimensional. The $\frac{2}{3}$-filled t_{2g} bands split into a wide xy and two narrow xz and yz bands, with bandwidth ratio $R = W_{xz/yz}/W_{xy} \sim 0.5$ and occupations n_{xy}, n_{xz}, and n_{yz}. Many-body studies of three-band Hubbard models have shown that a small R, a crystal-field splitting Δ, and a finite Coulomb exchange interaction can have a large impact on the electronic structure, leading in some cases to negative[16] orbital polarization $p = n_{xy} - (n_{xz} + n_{yz})/2$ and even to orbital-selective Mott transitions.[17,18] Infinite-layered ($n \to \infty$) systems are three dimensional. By increasing n, the effective dimensionality increases; $W_{xz/yz}$ approaches the xy-band width ($R \sim 1$), while, due to the change in both structure and lattice distortions, the crystal-field and the hopping integrals can be strongly modified; different parameter regimes can be reached. Furthermore, for real materials, there are indications that e_g states may also affect material properties.[6,19,20] The key parameters to determine are thus the crystal-field splittings in the Ru 4d shell, as well as the orbital occupations.

In this work we focus on the $Sr_{n+1}Ru_nO_{3n+1}$ series. The recent availability of high-quality $Sr_4Ru_3O_{10}$ single crystals, combined with comparably pure $Sr_3Ru_2O_7$ and Sr_2RuO_4 ones, allows us to reveal, for the first time, the evolution of the unoccupied electronic structure in the family. We use polarization-dependent O 1s x-ray-absorption spectroscopy (XAS) and analyze the spectra by means of *ab initio* and many-body methods. We find that, contrary to previous suggestions,[20,21] the splitting between e_g states is less than 1 eV, while, surprisingly, Sr bands are essential to understanding the spectra. We show that, at low energy, the main difference among the materials is a substantial rearrangement of t_{2g} orbital occupations. This rearrangement is controlled by the interplay of dimensionality, the t_{2g} crystal field, and Coulomb repulsion.

II. METHOD

High-quality $Sr_{1+n}Ru_nO_{3n+1}$ ($n = 1,2,3$) single crystals have been grown by the flux-feeding floating-zone technique, with Ru self-flux,[22] while exploiting recent advances in fabrication techniques.[22–24] The structure and crystalline qualities of the samples were assessed by a high-resolution x-ray diffractometer (Philips, model X' Pert MRD), with a Cu $K\alpha$ source. The x-ray-diffraction pattern taken on cleaved surface of Sr_2RuO_4, $Sr_3Ru_2O_7$, and $Sr_4Ru_3O_{10}$ crystals, shown in Fig. 2, confirm the absence of spurious phases. All the diffraction peaks can be identified with the expected (00l) Bragg reflections of the Sr-based Ruddlesden-Popper ruthenates structures. Absorption spectra at the O K edge were measured at the Beamline for Advanced Dichroism (BACH) at Elettra,[25] in the total-electron-yield mode[26] and at $T = 115$ K. All sample surfaces were prepared *in situ* by cleaving in a high ultravacuum. The O 1s XAS spectra for the three systems were acquired with fixed photon polarization and an incident angle θ_{inc} varying from 0° to 70°. The XAS data were normalized to the beam intensity at 560 eV, which is well above

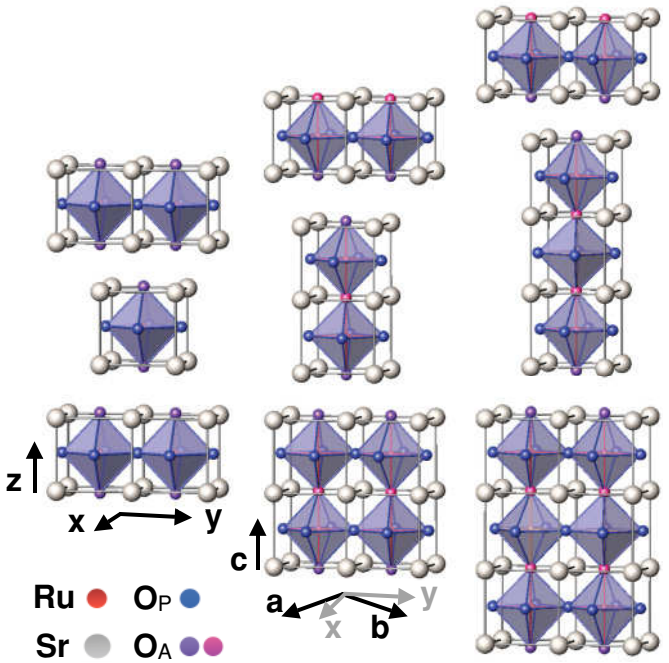

FIG. 1. (Color online) Left to right: Crystal structure of Sr_2RuO_4, $Sr_3Ru_2O_7$, and $Sr_4Ru_3O_{10}$.[1] The tetragonal (Sr_2RuO_4) and pseudotetragonal[2] ($Sr_3Ru_2O_7$ and $Sr_4Ru_3O_{10}$) axes are indicated by **x**, **y**, and **z**.

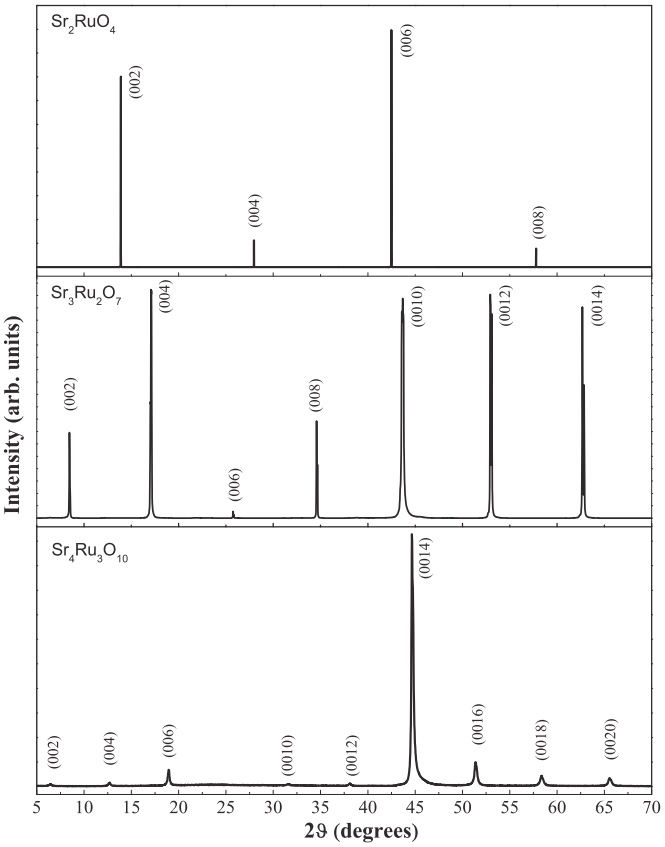

FIG. 2. X-ray-diffraction patterns of a cleaved (001) surface of Sr_2RuO_4, $Sr_3Ru_2O_7$, and $Sr_4Ru_3O_{10}$ crystals, grown with the flux-feeding floating-zone method. The spectra show the absence of any spurious phase and all the peaks are indexed as (00l) peaks of the Sr-based Ruddelsden-Popper ruthenates structures.

the absorption threshold $E_0 \sim 528$ eV. The incoming-photon electric field $\vec{E}$ has an in-plane component $E_{xy} = |\vec{E}| \cos\theta_{\rm inc}$ and an out-of-plane component $E_z = |\vec{E}| \sin\theta_{\rm inc}$, parallel to the **c** axis. Due to the dipole selection rules, the in-plane field induces O $1s \rightarrow$ O $2p_{x/y}$ excitations only, while the out-of-plane field induces exclusively O $1s \rightarrow$ O $2p_z$ transitions. Thus, by changing $\theta_{\rm inc}$, empty states with different symmetries are probed.

In order to identify the electronic states we first compare the experiments with *ab initio* calculations based on the local-density approximation (LDA). For Sr_2RuO_4 and $Sr_3Ru_2O_7$ we compare our LDA bands with published band structures[19,27] and find good agreement. In the next step we use the down-folding technique based on the Nth-order muffin-tin orbital method to construct material-specific Wannier functions that span the Ru 4d bands; we then obtain hopping integrals and crystal-field splittings.[28] Finally, for relevant cases, from these Wannier functions we build material-dependent t_{2g} Hubbard models and solve them using the dynamical mean-field theory (DMFT), within the LDA+DMFT approach.[29] We adopt the LDA+DMFT implementation discussed in Ref. 2, which is based on a weak-coupling continuous-time quantum Monte Carlo solver.[30]

III. RESULTS

The XAS spectra for horizontal polarization are shown in Fig. 3. There are two main absorption regions: a low-energy one that extends from E_0 to $E_1 = 530$ eV and a high-energy one from E_1 to $E_2 = 536$ eV. In the low-energy region, Sr_2RuO_4 exhibits a double-peak structure (A and B features), which can be ascribed[31] to the energy difference between apical (O_A) and planar (O_P) oxygen 1s core levels. The double peak turns into a single peak with a shoulder in $Sr_3Ru_2O_7$ and $Sr_4Ru_3O_{10}$. The energy separation between peaks B and C is about 4 eV in Sr_2RuO_4 and slightly increases to $n = 2,3$, mainly because the feature C drifts to higher energy. The spectral weight between B and C increases as n grows. In all systems, a progressive spectral weight transfer from the high- to the low-energy region is observed by increasing $\theta_{\rm inc}$ from 0° to 70°. Finally, for 0°, peak C is considerably reduced for the bilayered and trilayered materials.

For horizontal polarization, the XAS intensity can be estimated[32] as $I(\theta_{\rm inc},\omega) = \frac{1}{2}[\rho_x(\omega) + \rho_y(\omega)]\cos^2\theta_{\rm inc} + \rho_z(\omega)\sin^2\theta_{\rm inc}$. The factors $\rho_\alpha(\omega) = \sum_i \rho_{\alpha i}(\omega - \epsilon_i^{1s})$, with $\alpha = x,y,z$, are sums of the orbital-resolved O density of empty states $\rho_{\alpha,i}(\omega - \epsilon_i^{1s})$, while $-\epsilon_i^{1s}$ is the 1s core energy (with respect to the Fermi level) of oxygen i. In Fig. 4 we compare XAS experiments with $I(\theta_{\rm inc},\omega)$ obtained from LDA calculations. The agreement with experiments is good in the full energy window. A crucial ingredient is the spread in O 1s core energies. In the case of Sr_2RuO_4 this amounts to a negative shift of ~ 1.3 eV of the planar (O_P) oxygen 1s level with respect to the apical (O_A) oxygen 1s level. For $Sr_3Ru_2O_7$ there are one planar and two nonequivalent apical oxygens (O_{A_1} and O_{A_2}); the core energy shifts are $\sim$0.8 eV (O_{A_2}) and $\sim$1.2 eV (O_P). Finally, for $Sr_4Ru_3O_{10}$ the apical oxygen

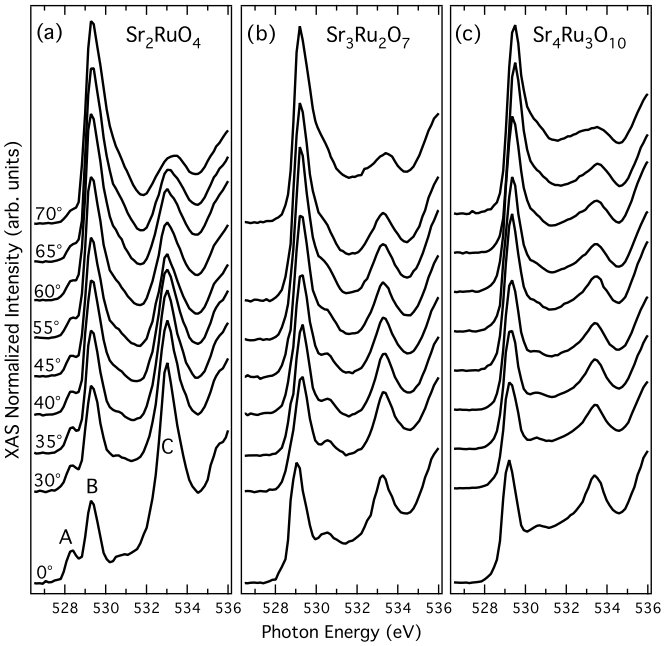

FIG. 3. XAS spectra ($T = 115$ K) at the O K edge for (a) Sr_2RuO_4, (b) $Sr_2Ru_3O_7$, and (c) $Sr_4Ru_3O_{10}$. The spectra are shown for several values of θ_{inc}, the angle between **c** and the incoming x rays. The cleaved surface is perpendicular to the **c** axis (Fig. 1). A, B, and C label the most relevant features.

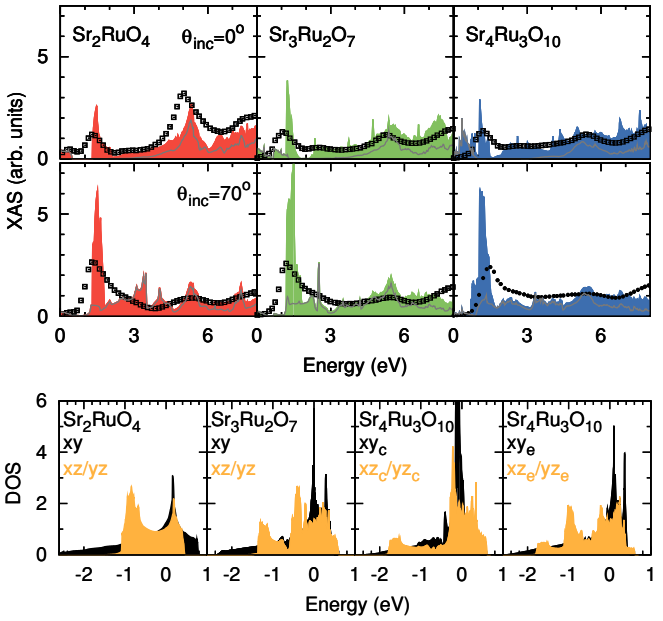

FIG. 4. (Color online) Top: XAS experimental da (open squares) and LDA results (filled curves) for $\theta_{inc} = 0°$ and 70°. The energy zero is the absorption threshold (E_0); the normalization is the number of atoms per cell. The gray lines show the apical oxygen contribution. Bottom: t_{2g} density of states (states/eV) per Ru site. For $Sr_4Ru_3O_{10}$ both central Ru (c) and external Ru (e) contributions are shown. Energy zero is denoted by ε_F.

core-energy shifts are ∼0–0.4 eV while the planar ones are ∼0.7–1.1 eV.[33]

Given the good agreement between LDA results and experiments, we proceed to the identification of the electronic states. We start with the analysis of the low-energy-absorption region. Figure 4 shows that at the absorption threshold (feature A in Sr_2RuO_4) the main contribution comes from O_A, while peak B is mainly due to O_P. We find that in this energy window O p electrons hybridize mostly with Ru t_{2g} electrons.

In the case of Sr_2RuO_4 W_{xy} is considerably larger than $W_{xz/yz}$; the ratio $R \sim 0.5$. The highest-energy crystal-field Wannier orbital is $|xy\rangle$; the $|xz\rangle$ and $|yz\rangle$ Wannier states are degenerate and $\Delta \equiv E_{xz/yz} - E_{xy} \sim -60$ meV. The orbital polarization $p_{LDA} \sim -0.35$. The xz and yz orbitals mostly hybridize with O_A x and y and O_P z, while xy orbitals hybridize with O_P x and y. Thus, for $\theta_{inc} = 0°$, feature A mainly originates from the xz and yz bands, while peak B comes from the xy band. With increasing θ_{inc} the contribution of $\rho_x + \rho_y$ decreases, while that from ρ_z increases. Thus peak A progressively decreases, while peak B changes its character from xy to xz/yz. This assignment is in agreement with previous works.[20,21,31] The ratio $I(70°,\omega)/I(0°,\omega)$ is small for peak A because the contribution from O_A z states is tiny; however, the ratio is ∼ 2–3 for peak B because xy and $xz + yz$ states couple to the same number of O_P states and $R \sim 0.5$.

In the case of $Sr_3Ru_2O_7$ and $Sr_4Ru_3O_{10}$, due to the large spread in core-energy shifts, peak A splits and appears only as a shoulder of peak B, while, in the latter, the xz/yz and xy features partially overlap even for $\theta_{inc} = 0°$. This leads to a line-shape modification of peak B and, for $Sr_4Ru_3O_{10}$, an energy shift of the maximum of ∼0.4 eV with increasing θ_{inc} from 0° to 70° (Fig. 3). $W_{xz/yz}$ rapidly increases and the bandwidth ratio approaches the infinite layers limit: $R \sim 0.7$ in $Sr_3Ru_2O_7$ and $R \sim 0.8$ in $Sr_4Ru_3O_{10}$. The crystal-field orbitals are affected by the structural changes. Crucial aspects are changes not only in RuO bonds but also in SrRu and SrO distances and in the Sr cage. In the case of $Sr_3Ru_2O_7$ we find that the lowest-energy orbital is $|xy\rangle$ and $\Delta \sim 45$ meV. The orbital polarization increases with respect to Sr_2RuO_4: $p_{LDA} \sim -0.05$. In $Sr_4Ru_3O_{10}$ there is a distribution of small splittings, with $\Delta \sim 120$ meV for the Ru in the central layers and $\Delta \sim -90$ meV for the Ru in the external ones. Correspondingly, the total polarization $p_{LDA} \sim 0$, with $p_{LDA} \sim 0.5$ for the central layer and $p_{LDA} \sim -0.25$ for the external layers.

Our results show that at low energy the most significant difference among the three systems is the rearrangement of t_{2g} orbital occupations. We find that this rearrangement stems from the interplay between the dimensionality and the t_{2g} crystal field and it is associated with a change in the position of the Fermi level ε_F in the density of states (DOSs) (Fig. 4). At $\frac{2}{3}$ filling, a small ratio R ($n = 1$) favors the occupation of the xz and yz states ($p < 0$), while a large positive Δ favors the occupation of the xy states ($p > 0$) (Ref. 2) and eventually pushes the xy-band van Hove singularity (ε^{xy}_{vHS}) to the left of ε_F. For $n \to \infty$, in the absence of distortions, $R \to 1$, $p \to 0$, and $\varepsilon_F \to \varepsilon^{xy}_{vHS}$; the effects of the crystal field and distortions, however, become progressively stronger. In Sr_2RuO_4, $\Delta \sim -60$ meV; a positive $\Delta \sim 60$ meV would yield a small $p \sim 0.1$, $\varepsilon_F \sim \varepsilon^{xy}_{vHS}$, and $\rho_{xz/yz}(\varepsilon_F)$ with positive curvature (favorable to metamagnetism[34]). For $n = 2,3$ we find that the calculated crystal field already yields a small or positive polarization and $\varepsilon_F \sim \varepsilon^{xy}_{vHS}$. Thus, while the actual position of ε_F depends on the details, ferromagnetic and

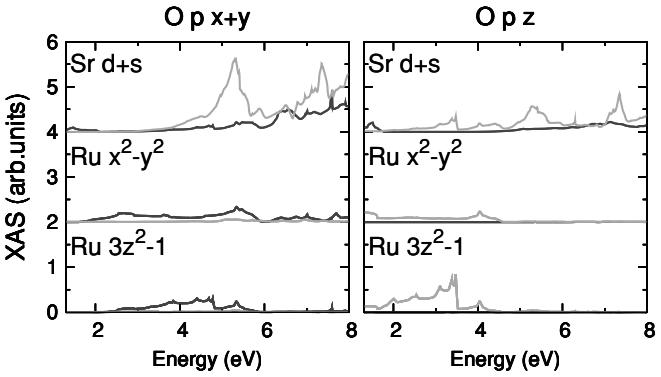

FIG. 5. Sr_2RuO_4: Sr $d+s$ and Ru e_g contributions to the XAS intensity (Fig. 4). The dark gray curves show O_PXAS (with a 1.3-eV shift) and the light gray curves show O_AXAS. $E_0 = 0$. Left: O x and y. Right: O z.

metamagnetic instabilities appear to be more likely with an increasing number of layers n.

Electronic-correlation effects can modify orbital occupations.[35] To evaluate such effects we perform many-body LDA+DMFT calculations for the three-band Hubbard models constructed from the t_{2g} Wannier functions. We take as parameters $U = 3.1$ eV and $J = 0.7$ eV, in line with theoretical estimates.[2,36] We find that p is somewhat smaller than in the LDA: At 290 K, $p_{\mathrm{DMFT}} \sim -0.11$ for Sr_2RuO_4 and $p_{\mathrm{DMFT}} \sim 0$ for $Sr_3Ru_2O_7$. Thus, due to many-body effects, holes are partially transferred from the xy bands to the xz and yz bands;[16] however, down to 290 K the trend remains the same as in the LDA.

Let us now analyze the high-energy-absorption region. For Sr_2RuO_4, the Ru and Sr contributions to the XAS are shown in Fig. 5. We find that e_g holes contribute right below 530 eV and extend to the full high-energy sector. The t_{2g}-e_g crystal-field splitting is about 3.4–3.5 eV in all materials, in line with previous estimates,[20] while the splitting within e_g states[37] is 0.7 eV in Sr_2RuO_4 and 0.3 eV or smaller in $Sr_3Ru_2O_7$ and $Sr_4Ru_3O_{10}$, i.e., considerably less than the surprisingly large values (∼2–3 eV) previously inferred from XAS data.[20,21] In Sr_2RuO_4, Ru $3z^2 - 1$ states contribute the most between 529 and 532 eV, through coupling to O_A z, and between 531 and 534 eV, through coupling to O_P x and y (Fig. 5). By increasing the number of RuO_2 layers the $3z^2 - 1$ band becomes broader, so that its contribution spreads to a larger-energy window. Ru $x^2 - y^2$ bands contribute the most, for all three materials, between 530 and 535 eV, through coupling to O_P x and y. The coupling to apical O z states is small (but not zero) around 532 eV, in line with previous suggestions.[20]

Sr states also hybridize with O p orbitals. Remarkably, they start to be relevant at 531 eV, as Fig. 5 shows. In Sr_2RuO_4, Sr xz and yz strongly contribute to peak C, mainly through hybridization with x and y of the neighboring O_A along **c** (Fig. 5, top left); this leads to a revision of previous interpretations,[20,21] which ascribed peak C only to Ru $x^2 - y^2$ states. When n increases the Sr contribution decreases, as only atoms in the external layers couple to apical x and y.

IV. CONCLUSION

In conclusion, by combining XAS with *ab initio* and many-body calculations, we understand basic aspects of the electronic structure of the $Sr_{n+1}Ru_nO_{3n+1}$ series. We found that the splitting within e_g states is less than 1 eV, similarly to $3d$ transition-metal oxides, and, surprisingly, Sr d bands are crucial to understanding the XAS spectra. These conclusions are likely to apply to all Sr and Ca layered $4d$ perovskites of the Ruddlesden-Popper family. Finally, we have shown that, due to the interplay among dimensionality, the t_{2g} crystal field, and Coulomb repulsion, there is a substantial rearrangement of the t_{2g} orbital occupation in the series. This reflects a shift in the position of the van Hove singularities close to the Fermi level, which could explain[19,34] the increased tendency to ferromagnetism and metamagnetism for $n = 2,3$ and could be the root[8,34] of the diversity of behaviors in the family.

ACKNOWLEDGMENTS

E.G. and E.P. acknowledge the Jülich BlueGene/P Grant No. JIFF41, as well as financial support by the Deutsche Forschungsgemeinschaft through the research unit FOR 1346.

*Present address: Department of Physics, University of Johannesburg, P.O. Box 524, Auckland Park 2006, South Africa.
†e.pavarini@fz-juelich.de
‡mario.cuoco@cnr.it

[1] H. Shaked, J. D. Jorgensen, O. Chmaissem, S. Ikeda, and Y. Maeno, J. Solid State Chem. **154**, 361 (2000); M. K. Crawford, R. L. Harlow, W. Marshall, Z. Li, G. Cao, R. L. Lindstrom, Q. Huang, and J. W. Lynn, Phys. Rev. B **65**, 214412 (2002).
[2] E. Gorelov, M. Karolak, T. O. Wehling, F. Lechermann, A. I. Lichtenstein, and E. Pavarini, Phys. Rev. Lett. **104**, 226401 (2010).
[3] Y. Maeno, H. Hashimoto, K. Yoshida, S. Nishizaki, T. Fujita, J. G. Bednorz, and F. Lichtenberg, Nature (London) **372**, 532 (1994); A. P. Mackenzie and Y. Maeno, Rev. Mod. Phys. **75**, 657 (2003).
[4] M. Neupane, P. Richard, Z.-H. Pan, Y.-M. Xu, R. Jin, D. Mandrus, X. Dai, Z. Fang, Z. Wang, and H. Ding, Phys. Rev. Lett. **103**, 097001 (2009).
[5] S. Nakatsuji, D. Hall, L. Balicas, Z. Fisk, K. Sugahara, M. Yoshioka, and Y. Maeno, Phys. Rev. Lett. **90**, 137202 (2003).
[6] A. Tamai, M. P. Allan, J. F. Mercure, W. Meevasana, R. Dunkel, D. H. Lu, R. S. Perry, A. P. Mackenzie, D. J. Singh, Z.-X. Shen, and F. Baumberger, Phys. Rev. Lett. **101**, 026407 (2008).
[7] R. A. Borzi, S. A. Grigera, R. S. Perry, N. Kikugawa, K. Kitagawa, Y. Maeno, and A. P. Mackenzie, Phys. Rev. Lett. **92**, 216403 (2004).
[8] J. Lee, M. P. Allan, M. A. Wang, J. Farrel, S. A. Grigera, F. Baumberger, J. C. Davis, and A. P. Mackenzie, Nature Phys. **5**, 800 (2009).

[9]X. N. Lin, Z. X. Zhou, V. Durairaj, P. Schlottmann, and G. Cao, Phys. Rev. Lett. **95**, 017203 (2005).
[10]R. S. Perry, L. M. Galvin, S. A. Grigera, L. Capogna, A. J. Schofield, A. P. Mackenzie, M. Chiao, S. R. Julian, S. Ikeda, S. Nakatsuji, Y. Maeno, and C. Pfleiderer, Phys. Rev. Lett. **86**, 2661 (2001).
[11]R. A. Borzi, S. A. Grigera, J. Farrell, R. S. Perry, S. J. S. Lister, S. L. Lee, D. A. Tennant, Y. Maeno, and A. P. Mackenzie, Science **315**, 214 (2007).
[12]S. Grigera, R. S. Perry, A. J. Schofield, M. Chiao, S. R. Julian, G. G. Lonzarich, S. I. Ikeda, Y. Maeno, A. J. Millis, and A. P. Mackenzie, Science **294**, 329 (2001).
[13]G. Cao, L. Balicas, W. H. Song, Y. P. Sun, Y. Xin, V. A. Bondarenko, J. W. Brill, S. Parkin, and X. N. Lin, Phys. Rev. B **68**, 174409 (2003).
[14]Z. Q. Mao, M. Zhou, J. Hooper, V. Golub, and C. J. O'Connor, Phys. Rev. Lett. **96**, 077205 (2006).
[15]R. Gupta, M. Kim, H. Barath, S. L. Cooper, and G. Cao, Phys. Rev. Lett. **96**, 067004 (2006).
[16]For $\Delta \ll J$, limit values of the orbital polarization are $p = 1$ ($n_{xy} = 2$ and $n_{xz} + n_{yz} = 2$, as for the xy-orbital order) and $p = -1/2$ ($n_{xy} = 1$ and $n_{xz} + n_{yz} = 3$, as in the case of the orbital-selective Mott transition).
[17]V. Anisimov, I. A. Nekrasov, D. E. Kondakov, T. M. Rice, and M. Sigrist, Eur. Phys. J. B **25**, 191 (2002).
[18]L. de Medici, S. R. Hassan, M. Capone, and X. Dai, Phys. Rev. Lett. **102**, 126401 (2009).
[19]D. J. Singh and I. I. Mazin, Phys. Rev. B **63**, 165101 (2001).
[20]H.-J. Noh *et al*., Phys. Rev. B **72**, 052411 (2005).
[21]S. J. Moon *et al*., Phys. Rev. B **74**, 113104 (2006).
[22]Z. Q. Mao, H. Fukazawa, and Y. Maeno, Mater. Res. Bull. **35**, 1813 (2000); R. Fittipaldi, A. Vecchione, S. Fusanobori, K. Takizawa, H. Yaguchi, J. Hooper, R. S. Perry, and Y. Maeno, J. Cryst. Growth **271**, 152 (2004); R. Fittipaldi, D. Sisti, A. Vecchione, and S. Pace, Cryst. Growth Design **7**, 2495 (2007).
[23]R. Perry and Y. Maeno, J. Cryst. Growth **271**, 134 (2004).
[24]M. Zhou, J. Hooper, D. Fobes, Z. Q. Mao, V. Golub, and C. J. O'Connor, Mater. Res. Bull. **40**, 942 (2005).
[25]M. Zangrando, M. Finazzi, G. Paolucci, G. Comelli, B. Diviacco, R. P. Walker, D. Cocco, and F. Parmigiani, Rev. Sci. Instrum. **72**, 1313 (2001); M. Zangrando, M. Zacchigna, M. Finazzi, D. Cocco, R. Rochow, and F. Parmigiani, *ibid*. **75**, 31 (2004).
[26]The total-electron-yield O K-edge spectra measured in vertical polarization at different incidence angles (i.e., different penetration depths, varying in the range 2–10 nm) show basically no angular dependence. This indicates that the electronic structure at 2–3 nm already resembles that of the bulk and is the same as that probed in the fluorescence-yield mode. Reference 31 shows that for Sr_2RuO_4 the O K-edge total-electron-yield and fluorescence-yield spectra are indeed remarkably similar (including relative peak heights within one orientation) and the principal difference is the background. We obtained similar results in the cases we tested.
[27]D. J. Singh, Phys. Rev. B **52**, 1358 (1995); T. Oguchi, *ibid*. **51**, 1385 (1995); E. Pavarini and I. I. Mazin, *ibid*. **74**, 035115 (2006).
[28]E. Pavarini, S. Biermann, A. Poteryaev, A. I. Lichtenstein, A. Georges, and O. K. Andersen, Phys. Rev. Lett. **92**, 176403 (2004); E. Pavarini, A. Yamasaki, J. Nuss, and O. K. Andersen, New J. Phys. **7**, 188 (2005).
[29]V. I. Anisimov, A. I. Poteryaev, M. A. Korotin, A. O. Anokhin, and G. Kotliar, J. Phys. Condens. Matter **9**, 7359 (1997); A. I. Lichtenstein and M. I. Katsnelson, Phys. Rev. B **57**, 6884 (1998).
[30]A. N. Rubtsov, V. V. Savkin, and A. I. Lichtenstein, Phys. Rev. B **72**, 035122 (2005).
[31]M. Schmidt, T. R. Cummins, M. Burk, D. H. Lu, N. Nucker, S. Schuppler, and F. Lichtenberg, Phys. Rev. B **53**, R14761 (1996).
[32]The estimate is obtained by averaging the (horizontal) polarization and neglecting the radial part of the dipole element of the matrix.
[33]Somewhat larger energy shifts (but identical trends) are obtained if the O 2s electrons are treated as valence states.
[34]B. Binz and M. Sigrist, Europhys. Lett. **65**, 816 (2004); S. Raghu, A. Paramekanti, E.-A. Kim, R. A. Borzi, S. A. Grigera, A. P. Mackenzie, and S. A. Kivelson, Phys. Rev. B **79**, 214402 (2009); W.-C. Lee and C. Wu, *ibid*. **80**, 104438 (2009).
[35]E. Pavarini, E. Koch, and A. I. Lichtenstein, Phys. Rev. Lett. **101**, 266405 (2008); E. Pavarini and E. Koch, *ibid*. **104**, 086402 (2010).
[36]Z. V. Pchelkina, I. A. Nekrasov, Th. Pruschke, A. Sekiyama, S. Suga, V. I. Anisimov, and D. Vollhardt, Phys. Rev. B **75**, 035122 (2007).
[37]All states but Ru d are downfolded. For $n = 2,3$, due to the e_g-t_{2g} mixing, the splittings are slightly smaller if all states but the e_g are downfolded.